Volume 6, Issue 3, 2016, 1222-1228 ISSN 2069-5837

Biointerface Research in Applied Chemistry

www.BiointerfaceResearch.com

Original Research Article Open Access Journal

Received: 25.01.2016 / Revised: 25.03.2016 / Accepted: 26.03.2016 / Published on-line: 01.04.2016

Carboxymethyl chitosan/forsterite bone tissue engineering scaffolds: correlations between composition and physico-chemical characteristics

Ali Samadikuchaksaraei [1,2], Mazaher Gholipourmalekabadi [3], Behrouz Farhadihosseinabadi [3], Zahra Rezvani [4], Masoud Mozafari [4,*]

[1]Department of Tissue Engineering & Regenerative Medicine, Faculty of Advanced Technologies in Medicine, Iran University of Medical Sciences, Tehran, Iran
[2]Cellular and Molecular Research Center, Iran University of Medical Sciences, Tehran, Iran
[3]Biotechnology Department, School of Advanced Technologies in Medicine, Shahid Beheshti University of Medical Sciences, Tehran, Iran
[4]Bioengineering Research Group, Nanotechnology and Advanced Materials Department, Materials and Energy Research Center (MERC), Tehran, Iran
*corresponding author e-mail address: ***mozafari.masoud@gmail.com***

ABSTRACT

Although chitosan-based scaffolds have shown promising biological characteristics, their low mechanical properties have been always as a major challenge in load-bearing tissue engineering applications. The aim of this study was to enhance the mechanical and biological properties of carboxymethyl chitosan-based scaffolds with incorporation of forsterite nanoparticles. The three-dimensional porous carboxymethyl chitosan/forsterite scaffolds were successfully fabricated via freeze-casting and lyophilization techniques by adding various weight concentrations of the forsterite nanoparticles. The correlations between the forsterite nanoparticles content and final characteristics of the prepared scaffolds were investigated. The results showed that the scaffolds had interconnected porosity structures varying from 58 to 87% with semi-uniform shapes, and pores' diameters of 440 to 310 µm. Moreover, the evaluations showed a meaningful correlation between the forsterite content within the carboxymethyl chitosan matrix and the mechanical and biological properties of the scaffolds. The scaffolds showed suitable compressive mechanical properties due to well-dispersion of forsterite nanoparticles. The results also indicated that all the prepared scaffolds did not change the cell viability of the human osteoblast-like cells and had no cytotoxic effect on the cells. Actively attachment of the cells to the scaffolds indicated a favorable cell adhesion property. All the data obtained from this study as well as desired shapes and simplicity of production suggest the potential use of carboxymethyl chitosan/forsterite nanocomposite scaffolds for bone tissue engineering.

KEYWORDS: *Tissue Engineering; Scaffold; Bone; carboxymethyl chitosan*

1. INTRODUCTION

Many ailments such as trauma, diseases and tumors lead to bone lesions. Unlike small bone fractures, the bone defects with size of at least 6 mm in diameter somehow lead to loss of original structure and function of bone. These critical-sized bone defects are considered as one of the major problems in the science of orthopedics [1-3]. Tissue engineering, as an alternative approach, aims to restore the damaged tissues and their functionality through using three-dimensional (3D) scaffolds [4-8]. The implantation of such constructs in the defected bone is one of the promising strategies in bone tissue engineering [9-11].

A scaffold provides suitable physical and chemical frameworks to which the cells are attached, differentiated, and ultimately new tissues are formed. Therefore, success in designing of an ideal scaffold profoundly depends on its physic-chemical properties. A suitable scaffold for bone tissue regeneration is required to mimic all aspects of a natural bone such as chemical compositions, mechanical property, porosity, bioactivity and biocompatibility [12, 13]. A scaffold with promising characteristics for using as a bone substitute allows cell proliferation, ingrowth, differentiation and ultimately bone formation.

Bone, as a natural composite, consists of two phases of organic and mineral compounds. Therefore, significant attentions have been paid to the fabrication of polymer/ceramic nanocomposites in which the polymer and ceramic parts play as organic and mineral components of the scaffold, respectively [11, 14]. Having more than one component endows the nanocomposites a high ability to mimic the extracellular matrix (ECM) of a specific tissue [15, 16]. To date, many synthetic and natural biomaterials have been proposed for bone tissue engineering applications with different ranges of advantages and disadvantages to the market. However, many of these biomaterials are not still fully satisfactory. A wide range of polymers have been used for the fabrication of bone tissue scaffolds, among which chitosan has been extensively investigated for various tissue engineering applications due to its nontoxic, non-antigenic and biodegradable properties as well as anti-microbial activities. Furthermore, chitosan is a hydrophilic biodegradable polymer due to the presence of hydroxyl groups on its backbone. In addition, this biomaterial has high cell adhesion property and biocompatibility [17]. In spite of the great number of successful applications, low mechanical properties and non-bioactivity of chitosan has remained challenging [18-20]. The problems observed in pure chitosan scaffolds can be minimized with the incorporation of a wide range of ceramic-based biomaterials such as hydroxyapatite, bioactive glasses, forsterite, etc. [21, 22]. Forsterite (Mg_2SiO_4), as a novel bioceramic, has a superior mechanical property in comparison with conventional calcium

phosphate based bioceramics [23-25]. Forsterite has also a remarkable osteoconductivity and osteoinductivity because of its ability in release of magnesium and silicon into the biological microenvironment in a controlled manner [26, 27]. Similar to other types of bioceramics such as hydroxyapatite and bioactive glasses, forsterite is bioactive and biocompatible [23-25]. In addition to bioactivity and biocompatibility, it is expected that incorporation of forsterite nanoparticles within the carboxymethyl chitosan matrix could remarkably enhance the mechanical properties of the scaffolds [28, 29].

The aim of this study was to prepare a 3D porous nanocomposite scaffolds based on carboxymethyl chitosan and various weight percentages of forsterite nanocrystals for bone tissue engineering applications. The correlations between the content of forsterite nanocrystals and the mechanical properties, microstructure, porosity as well as biological behavior of the resulted scaffolds was determined.

2. EXPERIMENTAL SECTION

2.1. Preparation of nanocrystalline forsterite.

Briefly, a transparent sol was prepared by dissolving 0.0142 mol magnesium nitrate (3.639 g) in 50 ml of de-ionized water. Next, 0.0071 mol of silica (1.642 g of colloidal silica) was introduced into the solution to set MgO/SiO2 molar ratio to 2:1 which corresponds to the theoretical value of pure forsterite. As the second solution, 0.0568 mol (19.426 g) sucrose was added into 100 ml of de-ionized water. Then, two solutions were mixed together and continuously stirred for 2 h. In the next step, 0.0071 mol (0.312 g) of PVA was mixed with 20 ml of de-ionized water to prepare a PVA solution and then added into the final solution and pH adjusted to 1 by drop-wise addition of diluted nitric acid, and finally the mixture stirred for 4 h. With the aim of letting the Mg2+ ions to react with sucrose completely the solution heated at 80 °C for 2 h on a hot plate stirrer, and then heated in an electric oven at 200 °C for complete dehydration and changing into a viscous dark brownish gel. Subsequently, the obtained mass was milled into a fine powder by planetary milling. After grinding and sieving, the dry powder calcined for 3 h at 900 °C.

2.2. Preparation of nanocomposite scaffolds.

Carboxymethyl chitosan (Mw=2.5×105, degree of deacetylation= 90%) and acetic acid were purchased from Aldrich Sigma (USA). Phosphate-buffered saline (PBS, 0.1 M, pH 7.4) was analytical grade and used as received. The carboxymethyl chitosan was first dissolved with concentrations of 2.0 wt % in 2.0% (v/v) acetic acid into deionized water. The mass ratio of forsterite powder in the carboxymethyl chitosan matrix was selected as 0, 10, 20, 30, 40 (wt%) by adding the powder into the polymeric solution to make a homogeneous mixture. The mixture was casted onto a mold with 6 mm height and 3 mm diameter, and then embedded in nitrogen liquid to solidify the solvent. The solidified mixture was transferred into a freeze dryer at the temperature of -50 °C and pressure of 0.5 mmHg for at least 3 days to completely remove the solvent. The samples were then soaked in glutaraldehyde solution of 1% (w/v) for 24 h, and then carefully washed for the removal of the unreacted glutaraldehyde molecules.

2.3. Characterization.

2.3.1. Transmission electron microscopy (TEM) analysis.

TEM study was performed with the Philips CM120 operated at 100 kV. The morphology and size of the synthesized forsterite nanoparticles assessed using TEM. For TEM analysis, the nanoparticles were ultrasonically dispersed in ethanol for 15 min to form very dilute suspensions, and then few drops were deposited on the carbon-coated copper grids.

2.3.2. Porosity measurement.

The porosity of the scaffold was determined by the following equation [30]:

$$\text{Porosity}\% = 1 - \frac{\rho_{\text{scaffold}}}{\rho_{\text{component}}}$$

where ρscaffold and ρcompact are the densities of the prepared scaffold and bulk material, respectively. The density of the scaffold was evaluated from masses and volume measurements of the scaffolds.

2.3.3. Swelling index.

The dry scaffolds were first weighted accurately and placed into the 15ml tubes containing 10 ml PBS solution at 37º C. At predetermined time intervals (1, 3, 7, 14 and 21 day), the swollen scaffolds were weighed again, and the degree of the swelling was calculated by the following equation:

$$SI = [(W_{st} - W_d)/W_d] \times 100\%$$

Where Ws and Wd are the measured masses of swollen and dry scaffolds, respectively.

2.3.4. SEM analysis.

The morphology and pore size of the scaffolds were evaluated by Scanning Electron Microscope (SEM, EMITECH K450X, England). For this purpose, the samples were sputter coated with gold and then viewed under SEM at the acceleration voltage of 15 kV.

2.3.5. X-ray powder diffraction (XRD) analysis.

The samples were analyzed by XRD (Siemens-Brucker D5000 diffractometer). This instrument works with voltage and current settings of 40 kV and 40 mA respectively and uses Cu-Ka radiation (1.540600 Å). For qualitative analysis, XRD diagrams were recorded in the interval $10° \leq 2\theta \leq 50°$at scan speed of 2°/min being the step size 0.02° and the step time 1 s.

2.3.6. Fourier transform infrared spectroscopy (FTIR) analysis.

The chemical bonds and compositions of the synthesized sample was performed by FTIR (Bomem MB 100 spectrometer). For IR analysis, in first 1 mg of material scarped from forsterite surface was carefully mixed with 300 mg of KBr (infrared grade) and palletized under vacuum. Then the pellets were analyzed in the range of 500 to 4000 cm^{-1} at the scan speed of 23 scan/min with 4 cm^{-1} resolution.

2.3.7. Mechanical behavior.

The mechanical behavior of the scaffolds was studied by using instrument (Roel-Amstel) following the guideline of ASTM F 451-86. The cylindrical samples were cut to an appropriate size

(3 mm in diameter and 6 mm in thickness) and conducted with a drawing rate of 1 mm/min.

2.4. Cellular response.

The in vitro biocompatibility and cell adhesion properties of the scaffolds were studied by culturing the SaOS-2 cell line (human osteoblast-like cells) (National Cell Bank of Iran, Pasture Institute) on the scaffolds with different concentrations of the forsterite. For this purpose, the cells were kept in Dulbecco's Modified Eagle Medium (DMEM) supplemented with 10% fetal bovine serum (FBS) and streptomycin/penicillin 100 U/mL (1%). For in vitro cellular response to the scaffolds, the cells were trypsinized, centrifuged and resuspended in a complete culture medium. A 200 µl of the cell suspension (1.5×106 cells.ml-1) were carefully seeded on top of each sample pre-soaked in the medium. The cell/scaffold constructs were then incubated at 37 °C in a humidified atmosphere of 95% air and 5% CO2.

2.4.1. Cell viability and cytotoxicity.

The effects of the scaffolds on cell proliferation and cytotoxicity were evaluated by MTT test and lactate dehydrogenase (LDH) activity assay, respectively. MTT test was carried out by a previously described protocol [31]. Briefly, the cells were seeded on the scaffold for 24, 48 and 72 hours. After the prescribed time points, the cell/scaffold complexes were washed with PBS. The samples were then treated with 15% MTT solution (5 mg.ml-1) in DMEM for 2 h at 37 °C. The optical density value of the samples was measured using an ELISA (enzyme-linked immunosorbent assay) reader at a wavelength of 590 nm with a reference filter of 620 nm after 30 min of DMSO treatment. The cells cultured in cell culture plate served as positive control (100% cell viability). The data was normalized to the positive control. All the data obtained from MTT assay was expressed as means ± standard deviation (SD) for n = 6. LDH activity in the cell culture medium was measured after 24, 48 and 72 hours of cell culturing. For this purpose, the medium was collected and centrifuged. LDH specific activity in the supernatant was measured for each time point by a LDH kit (ZistShimi kits, Co No: 10-503 and 10-533-1), based on P-Nitro Phenyl Phosphate conversion to P-Nitro Phenol. The UV absorbance of NADH, as an index of NADH concentration, was quantitated on a Biotek EL800 absorbance plate reader at 490 nm. At the same time, all the cells in the culture plate were ruptured by freeze-thawing and the data was normalized for total LDH activity of the 3×105 cells [32].

2.4.2. Cell adhesion.

The morphology of the SaOS-2 cells cultured on the scaffolds was observed by SEM. For this purpose, the cells were cultured on the scaffolds and maintained for 72 hours as described above. The samples were prepared for taking SEM micrographs by a protocol described in our previously published work [11]. Briefly, the samples were washed twice with PBS and fixed with 2.5% glutaraldehyde (GA) for 1 h. Post-fixation was carried out in 1% osmium tetroxide and dehydration in a graded acetone series solutions. The scaffolds were then freeze-dried and kept dry using silica gel until taking the SEM micrographs. The cell/scaffold constructs were coated with gold by sputtering and the morphology of the cells was viewed by SEM at the acceleration voltage of 15 kV.

2.5. Statistical analysis.

All experiments were performed at least in four replicate. The normal distribution of the groups was investigated by a Kolmogorov–Smirnov test. The data was analyzed statistically by one-way ANOVA and Tukey's test, where appropriate. The results were expressed as mean ± standard deviation. A P value of < 0.05 was defined as the level of significance. The SigmaPlot 11.0 θ software was used for plotting the graphs.

3. RESULTS SECTION

3.1. FTIR and TEM of forsterite nanoparticles.

FTIR analysis was used to determine the chemical bonds and compositions of the synthesized forsterite nanoparticles, shown in Figure 1 (a). As can be seen in this figure, the synthesized sample exhibited the main characteristic bands of ideal forsterite (Mg2SiO4) [33].

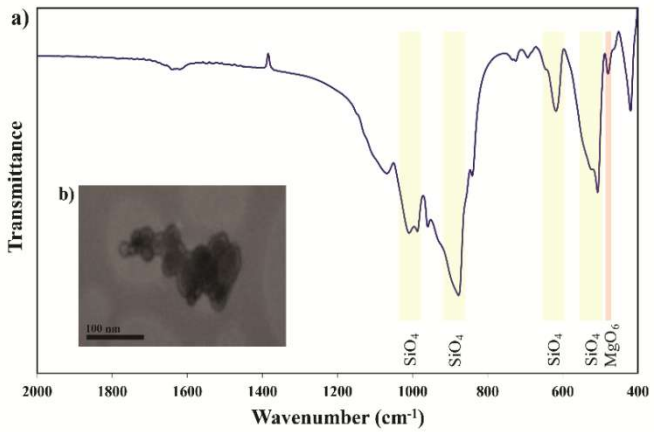

Figure 1. (a) FTIR analysis, and (b) TEM image of the synthesized forsterite nanoparticles.

For instance, the bands related to the characteristic peaks of forsterite appeared at 479 and 621 cm-1 for SiO4 bending, at 896 and 1008 cm-1 for SiO4 stretching and at 441 cm-1 for modes of octahedral MgO6. It is also worth to note that our obtained results were similar to the previous studies [34]. In addition, TEM was used to determine the morphology of the synthesized forsterite nanoparticles. Figure 1 (b) shows the TEM image of the synthesized forsterite nanoparticles after the final heat-treatment process, indicating that the particles were nearly in an elliptical shaped morphology and the size was less than 50 nm.

3.2. SEM observations.

The morphology of the carboxymethyl chitosan/forsterite scaffolds was studied by SEM and the outcome illustrated in Figure 2. As can be seen, the carboxymethyl chitosan-based scaffold showed a well-developed porous microstructure with a promising interconnectivity. With the increase of the forsterite content up to 40%, shown in Figure 2 (d), the surface of the pores exhibited a rougher texture, suggesting that a non-homogeneous layer of the forsterite was deposited onto the pore walls. In fact, the microstructure of the pores changed with the increase of the forsterite content, and the porosity decreased correspondingly.

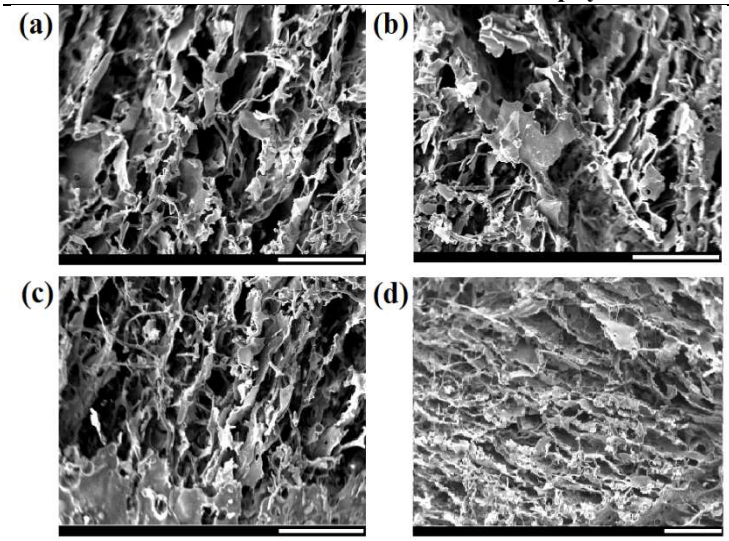

Figure 2. SEM micrographs of the prepared scaffold, (a-d) the mass ratio of forsterite nanoparticles in the carboxymethyl chitosan matrix was 0, 10, 20, 30, 40 (wt%), respectively. (The scale bar is 500 µm).

As can be seen, the porosity of the scaffolds depends on the content of forsterite particles used in composition. More generally, there is a correlation between the forsterite content and final characteristics of the scaffolds. It has been frequently reported that a typical scaffold for bone tissue engineering needs at least thirty present interconnected porosity to allow cell migration and cell ingrowth [35]. In addition, the porosity in spongy and compact bone found to be in ranges of 30-90% and 5-30%, respectively [36]. According to our results, the average porosity of the scaffolds without forsterite nanoparticles found to be around 86%, while with the impregnation of the forsterite nanoparticles up to 40% (w/v), the average porosity decreased to 59%. Therefore, all the prepared scaffolds showed porous structures similar to that of natural spongy bone. Different chitosan-based biomaterials have been used for the fabrication of 3D porous scaffolds [20, 37]. For example, Zhang et al. [37] fabricated porous chitosan-β-tricalcium phosphate (β-TCP) scaffolds from various contents of β-TCP, ranging 0-70% by a phase separation technique.

Table 1. Correlation between content of forsterite nanoparticles and pore parameters of the scaffolds.

Forsterite (Wt%)	Porosity (%)	Average pore size (µm)
Spongy bone	30-90% [36]	-
Compact bone	5-30% [36]	-
0	87±0.7	440
10	75±1.2	420
20	69±0.6	364
30	61±0.9	333
40	58±1.3	310

They showed that the porosity of the resulted scaffolds slightly decreased with an increase in the content of β-TCP up to 70% (88.89% and 85.71% porosities for 0% and 70% wt of the β-TCP, respectively). In this study, we also found that like porosity, the average pores' diameter decreased from 440 to 310 µm with the increase of forsterite content. The results of porosity and average pores' diameter of the scaffolds with different forsterite weight percentages are presented in Table. 1.

3.3. XRD.

The XRD patterns of the scaffolds containing different concentrations of forsterite is shown in Fig. 3. The XRD peaks of the samples showed typical peaks of carboxymethyl chitosan and forsterite nanoparticles, in which by increasing the amount of forsterite nanoparticles enhances its peaks intensities. As can be seen, the XRD patterns showed the existence of a single-phase pure forsterite in the structure of the scaffolds [38]. According to the JCPDS data file No. 34-0189, all the characteristic peaks of forsterite phase were obviously detected. The average nanocrystallite size was determined from the half-width of main diffraction peaks using the Debye-Scherrer's formula, estimated approximately 17 nm.

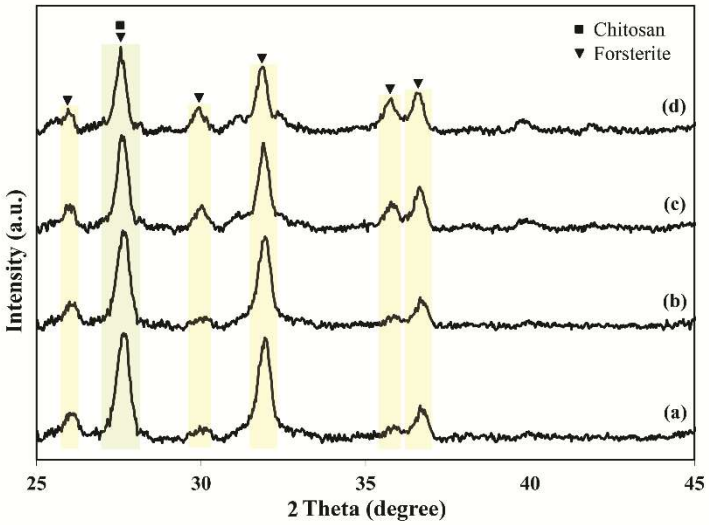

Figure 3. XRD patterns of the prepared scaffolds containing different amounts of forsterite. a) 10%, b) 20%, c) 30%, and d) 40%.

3.4. Mechanical properties.

Compressive strength has been conducted to determine the mechanical properties of the scaffolds after further addition of forsterite nanoparticles. Low mechanical property of porous chitosan-based constructs has remained a major challenging issue in using this type of biomaterial for bone tissue engineering scaffolds [39, 40]. Many attempts have been made to reinforce chitosan-based scaffolds with bioceramic materials [37, 41, 42]. For example, Zhang et al. [37] successfully reinforced a chitosan matrix with calcium phosphate to overcome the low biocompatibility of the pure chitosan scaffolds. Figures 4 (a) and 6 (b) give the results obtained from mechanical compressive tests of the samples. According to the results, the values of elastic modulus (E) and compressive strength (σ) significantly enhanced with the increased percentage of the forsterite.

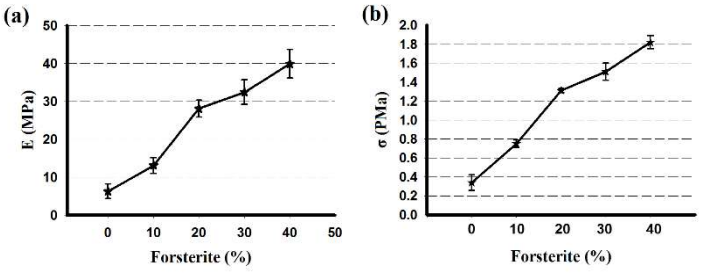

Figure. 4. The mechanical compressive tests of the samples, showing the values of elastic modulus (E) and compressive strength (σ) with the increase of forsterite content.

Correspondingly, the forsterite nanoparticles reinforced the polymeric matrix and enhanced the mechanical property of the scaffolds. It has been reported that E and σ for spongy bone are

20-500 and 4-12 MPa, respectively, while these parameters are increased to 3–30 × 103 and 130-180 MPa for compact bone. Therefore, the results indicated that the mechanical characteristics of the all scaffolds were nearly close to natural spongy bone [36, 43].

3.5. Swelling index.

Swelling index is an important parameter which can influence the chemical and physical characteristics of tissue engineering scaffolds. Herein, the swelling index of the prepared scaffolds was determined after five incubation times of 1, 3, 7, 14 and 21 days. The dependency of swelling index of the scaffolds on the weight percentage of the forsterite is presented in Figure 5. As can be seen, it is found that the swelling index decreased by the addition of the weight percentage of the forsterite content to the matrix. It is generally accepted that the scaffolds with higher porous structures provide more surface areas as well as higher water absorption. Additionally, chitosan compounds have frequently shown a high hydrophilic property [44, 45]. Therefore, both porosity and content of forsterite could affect the swelling index of the scaffolds. As mentioned before, porosity of the scaffolds slightly decreased when the content of the forsterite increased up to 40%. On the other hand, the decrease in the ratio of the carboxymethyl chitosan in the resulted scaffolds could profoundly decrease the swelling index [46]. As can be seen, the pure carboxymethyl chitosan construct had the highest swelling percentage in all the predetermined time periods.

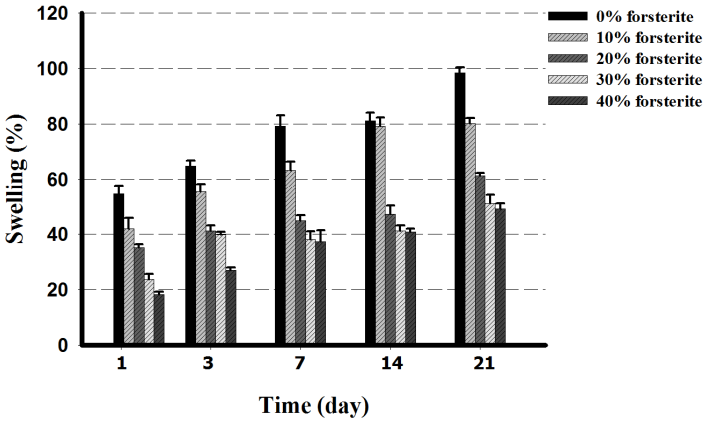

Figure. 5. The correlation between the swelling index of the scaffolds and the weight percentage of the forsterite nanoparticles.

3.6. *In vitro* cellular responses to scaffold.

The SaOS-2 cells have been frequently used in order to study the events associated with the late osteoblastic differentiation stages in human. These cells could deposit a mineralization-competent ECM [47, 48]. Therefore, the response of the cells to the scaffolds were investigated after culturing the cells within the scaffolds in vitro. The cell viability, cytotoxicity and cell adhesion properties of the scaffolds were evaluated by MTT test, LDH activity assay and SEM micrographs, respectively.

3.6.1. Cell viability and cytotoxicity.

The percentage of the cell viability was measured by MTT test based on mitochondrial metabolic activity of the living cells in reduction of the tetrazolium salt (MTT solution) into formazan [49, 50]. Figure 6a shows the MTT results of the scaffolds at three predetermined time points of 24, 48 and 72 hrs. The rate of cell proliferation slightly increased with the increase of forsterite content in the scaffolds, howbeit the differences were not statistically significant (one-way ANOWA, $p>0.05$). As mentioned above, both carboxymethyl chitosan and forsterite are biocompatible and non-cytotoxic [20, 26, 37]. Therefore, it is expected that the scaffolds synthesized from these materials have non-cytotoxicity property *in vivo*.

LDH enzyme, as a cellular enzyme that converts lactate to pyrovate, is released from ruptured or dead cells. It has been found that the measurement of LDH activity in cell culture medium is a simple and fast way for cytotoxicity evaluation [51]. The results obtained from LDH specific activity assay for each time point indicated that there was no significant difference between the amounts of released LDH between all the samples, as illustrated in Figure 6b. These findings showed that all the scaffolds (with and without forsterite nanoparticles) had a remarkable biocompatibility without any detectable cytotoxicity effects on the cells, which is in agreement with other studies [20, 26, 37, 52].

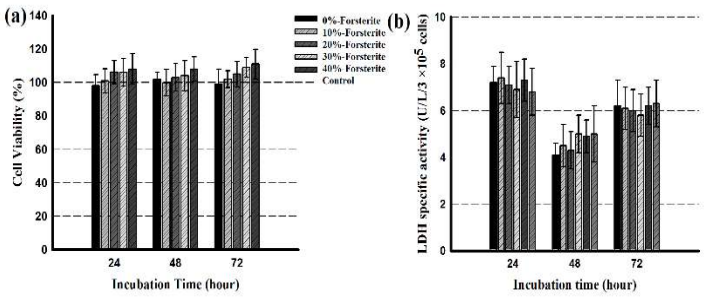

Figure. 6. (a) MTT results of the samples after three incubation times. The cell viability of the control was considered as 100%. No statistically significant change in viability of the cells was seen in comparison with control. (b) LDH activity of the cell/scaffold culture medium after three time points. There was not statistically significant difference between LDH specific activities of the samples and control sample ($p > 0.05$).

3.6.2. Cell adhesion.

In order to investigate the cell adhesion and cell-material interaction behavior, the SaOS-2 cells were propagated over the samples and observed for phenotypic properties under SEM observation. The SEM micrographs taken from 0% and 40% forsterite are shown in Figures 7a and 7b, respectively.

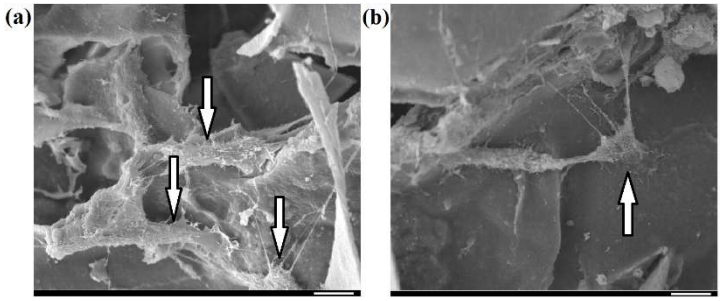

Figure. 7. SEM micrographs of the SaOS-2 cell line cultured on the scaffolds: a) 0%-forsterite and b) 40%- forsterite. The arrows show the cells grown on the scaffold. Scale bar = 10 µm.

As can be seen, the cells were attached actively to the scaffolds and spread on the porous scaffolds, indicating favorable cyto-compatible property of the samples that can allow the cell proliferation and adhesion [26, 45, 53, 54].

4. CONCLUSIONS

The present study has developed a strategy for the reinforcement of porous carboxymethyl chitosan scaffolds for bone tissue engineering applications. The correlation between the content of the forsterite in the prepared carboxymethyl chitosan/forsterite scaffolds was defined. The results showed remarkable effects due to the addition of the forsterite nanoparticles on the mechanical behavior of the scaffolds. The Young Modulus of the scaffolds was comparative to the natural spongy bone. Also, applying this type of scaffolds is notable from two points of view including the improved cell culture response and the favorable morphology and porosity of the scaffolds. Taken together, all the data obtained from this study support the potential application of forsterite-incorporated carboxymethyl chitosan scaffolds for bone tissue engineering.

5. REFERENCES

[1] Brighton C.T., Hunt R.M., Early histologic and ultrastructural changes in microvessels of periosteal callus, *Journal of orthopaedic trauma*, 11, 4, 244-253, **1997.**

[2] Ham A.W., Harris W.R., Repair and transplantation of bone, *The biochemistry and physiology of bone*, 3, 337, **1971.**

[3] Murugan R., Ramakrishna S., Development of nanocomposites for bone grafting, *Composites Science and Technology,* 65, 15-16, 2385-2406, **2005.**

[4] Moore W.R., Graves S.E., Bain G.I., Synthetic bone graft substitutes, *ANZ journal of surgery*, 71, 6, 354-361, **2001.**

[5] Dankers P.Y.W., Meijer E., Supramolecular biomaterials. A modular approach towards tissue engineering, *Bulletin of the Chemical Society of Japan,* 80, 11, 2047-2073, **2007.**

[6] Shoae-Hassani A., Differentiation of human endometrial stem cells into urothelial cells on a three-dimensional nanofibrous silk–collagen scaffold: an autologous cell resource for reconstruction of the urinary bladder wall, *Journal of tissue engineering and regenerative medicine*, 9**,** 11, 1268-1276, **2015.**

[7] Jafari J., Electrospun chitosan–gelatin nanofiberous scaffold: Fabrication and in vitro evaluation, *Bio-medical materials and engineering*, 21**,** 2, 99-112, **2011.**

[8] Van Vranken B.E., The differentiation of distal lung epithelium from embryonic stem cell, *Current protocols in stem cell biology*, 1G. 1.1-1G. 1.22, **2007.**

[9] Diba M., Preparation and characterization of polycaprolactone/forsterite nanocomposite porous scaffolds designed for bone tissue regeneration*, Composites Science and Technology*, **2012.**

[10] Goldstein A.S., Effect of convection on osteoblastic cell growth and function in biodegradable polymer foam scaffolds, *Biomaterials,* 22**,** 11, 1279-1288, **2001.**

[11] Mobini S., Bioactivity and biocompatibility studies on silk-based scaffold for bone tissue engineering*, Journal of Medical and Biological Engineering,* 33, 2, 207-214, **2013.**

[12] Collins M.N., Birkinshaw C., Hyaluronic acid based scaffolds for tissue engineering—A review, *Carbohydrate polymers*, 92, 2, 1262-1279, **2013.**

[13] Samadikuchaksaraei A., Bishop A.E., Effects of growth factors on the differentiation of murine ESC into type II pneumocytes, *Cloning and stem cells, 9*, 3, 407-416, **2007.**

[14] Gholipourmalekabadi M., In vitro and in vivo evaluations of three-dimensional hydroxyapatite/silk fibroin nanocomposites scaffolds, *Biotechnology and Applied Biochemistry*, **2014.**

[15] Jones J.R., Extracellular matrix formation and mineralization on a phosphate-free porous bioactive glass scaffold using primary human osteoblast (HOB) cells, *Biomaterials,* 28, 9, 1653-1663, **2007.**

[16] Hamlekhan A., Preparation of laminated poly (ε-caprolactone)-gelatin-hydroxyapatite nanocomposite scaffold bioengineered via compound techniques for bone substitution, *Biomatter,* 1, 1, 91, **2011.**

[17] Pillai C., Paul W., Sharma C.P., Chitin and chitosan polymers: Chemistry, solubility and fiber formation, *Progress in Polymer Science*, 34, 7, 641-678, **2009.**

[18] Madihally S.V., Matthew H.W., Porous chitosan scaffolds for tissue engineering, *Biomaterials,* 20, 12, 1133-1142, **1999.**

[19] Francis Suh J.-K., Matthew H.W., Application of chitosan-based polysaccharide biomaterials in cartilage tissue engineering: a review, *Biomaterials*, 21, 24, 2589-2598, **2000.**

[20] Zhang Y., Zhang M., Cell growth and function on calcium phosphate reinforced chitosan scaffolds, *Journal of Materials Science: Materials in Medicine*, 15, 3, 255-260, **2004.**

[21] Wawro D., Pighinelli L., Chitosan fibers modified with HAp/β–TCP nanoparticle, *International journal of molecular sciences*, 12, 11, 7286-7300, **2011.**

[22] Wang J., Evaluation of novel alginate dialdehyde cross-linked chitosan/calcium polyphosphate composite scaffolds for meniscus tissue engineering*, Carbohydrate Polymers*, 79, 3, 705-710, **2010.**

[23] Kharaziha M., Fathi M., Synthesis and characterization of bioactive forsterite nanopowder, *Ceramics International*, 35, 6, 2449-2454, **2009.**

[24] Kharaziha M., Fathi M., Improvement of mechanical properties and biocompatibility of forsterite bioceramic addressed to bone tissue engineering materials, *Journal of the mechanical behavior of biomedical materials*, 3, 7, 530-537, **2010.**

[25] Fathi M., Kharaziha M., Two-step sintering of dense, nanostructural forsterite, *Materials Letters*, 63, 17, 1455-1458, **2009.**

[26] Diba M., Preparation and characterization of polycaprolactone/forsterite nanocomposite porous scaffolds designed for bone tissue regeneration, *Composites Science and Technology*, 72, 6, 716-723, **2012.**

[27] Leng B., A comparative study of proliferation and osteogenic differentiation of rat adipose-derived stem cells in β-tricalcium phosphate (β-TCP), forsterite (Mg2SiO4) and clinoenstatite (MgSiO3), *Chinese Science Bulletin,* 58, 24, 3033-3042, **2013.**

[28] Correia C.O., Leite A.J., Mano J.F., Chitosan/Bioactive Glass Nanoparticles Scaffolds with Shape Memory Properties*, Carbohydrate Polymers,* **2015.**

[29] Jiang L., Preparation and properties of nano-hydroxyapatite/chitosan/carboxymethyl cellulose composite scaffold*, Carbohydrate Polymers,* 74, 3, 680-684, **2008.**

[30] Mano J., Natural origin biodegradable systems in tissue engineering and regenerative medicine: present status and some moving trends, *Journal of the Royal Society Interface*, 4, 17, 999-1030, **2007.**

[31] Gholipourmalekabadi M., Optimization of nanofibrous silk fibroin scaffolds as a delivery system for bone marrow adherent cells, *Biotechnology and applied biochemistry*, **2014.**

[32] Tahannejad Z., Dayer D., Samie M., The levels of Serum Alkaline Phosphatase and Lactate Dehydrogenase in Hodgkin Lymphoma, *Iranian Journal of Blood & Cancer,* 4, 3, 125-128, **2012.**

[33] Mozafari M., Synthesis and characterization of nanocrystalline forsterite coated poly (L-lactide-co-β-malic acid) scaffolds for bone tissue engineering applications, *Materials Science and Engineering: C*, **2015.**

[34] Libowitzky E., Beran A., OH defects in forsterite, *Physics and Chemistry of Minerals,* 22, 6, 387-392, **1995.**

[35] Wu C., Preparation of porous scaffolds in bone tissue engineering, *Chin J Clin Rehabil*, 8, 5, 929-931, **2004.**

[36] Murugan R., Ramakrishna S., Development of nanocomposites for bone grafting*, Composites Science and Technology*, 65, 15, 2385-2406, **2005.**

[37] Zhang Y., Zhang M., Synthesis and characterization of macroporous chitosan/calcium phosphate composite scaffolds for tissue engineering, *Journal of biomedical materials research*, 55, 3, 304-312, **2001.**

[38] Kamalian R., Synthesis and characterisation of bioactive glass/forsterite nanocomposites for bone and dental implants, *Ceramics-Silikáty,* 56, 4, 331-340, **2012.**

[39] Upadhyaya L., Biomedical applications of carboxymethyl chitosans, *Carbohydrate polymers,* 91, 1, 452-466, **2013.**

[40] Jayakumar R., Biomedical applications of chitin and chitosan based nanomaterials—A short review, *Carbohydrate Polymers*, 82, 2, 227-232, **2010.**
[41] Peter M., Novel biodegradable chitosan–gelatin/nano-bioactive glass ceramic composite scaffolds for alveolar bone tissue engineering, *Chemical Engineering Journal*, 158, 2, 353-361, **2010.**
[42] Peter M., Nanocomposite scaffolds of bioactive glass ceramic nanoparticles disseminated chitosan matrix for tissue engineering applications, *Carbohydrate Polymers*, 79, 2, 284-289, **2010.**
[43] Mozafari M., Biomimetic formation of apatite on the surface of porous gelatin/bioactive glass nanocomposite scaffolds, *Applied Surface Science,* 257, 5, 1740-1749, **2010.**
[44] Brine C.J., Sandford P.A., Zikakis J.P., Advances in chitin and chitosan,. **1992.**
[45] Khor E., Lim L.Y., Implantable applications of chitin and chitosan, *Biomaterials*, 24, 13, 2339-2349, **2003.**
[46] Gorczyca G., Preparation and characterization of genipin cross-linked porous chitosan–collagen–gelatin scaffolds using chitosan–CO 2 solution, *Carbohydrate polymers*, 102, 901-911, **2014.**
[47] McQuillan D., Richardson M., Bateman J., Matrix deposition by a calcifying human osteogenic sarcoma cell line (SAOS-2), *Bone*, 16, 4, 415-426, **1995.**
[48] Poursamar S.A., Azami M., Mozafari M., Controllable synthesis and characterization of porous polyvinyl alcohol/hydroxyapatite nanocomposite scaffolds via an< i> in situ</i> colloidal technique, *Colloids and Surfaces B: Biointerfaces*, 84, 2, 310-316, **2011.**
[49] Gholipourmalekabadi M., Detection and qualification of optimum antibacterial and cytotoxic activities of silver-doped bioactive glasses, *IET Nanobiotechnology*, **2015.**
[50] Rostami A., Optimization of fluoride-containing bioactive glasses as a novel scolicidal agent adjunct to hydatid surgery, *Acta tropica*, 148, 105-114, **2015.**
[51] Koh J.Y., Choi D.W., Quantitative determination of glutamate mediated cortical neuronal injury in cell culture by lactate dehydrogenase efflux assay, *Journal of neuroscience methods*, 20, 1, 83-90, **1987.**
[52] Wan Y., Porous polylactide/chitosan scaffolds for tissue engineering, *Journal of Biomedical Materials Research Part A*, 80, 4, 776-789, **2007.**
[53] Freier T., Controlling cell adhesion and degradation of chitosan films by< i> N</i>-acetylation, *Biomaterials*, 26, 29, 5872-5878, **2005.**
[54] Gholipourmalekabadi M., Decellularized human amniotic membrane: more is needed for an efficient dressing for protection of burns against antibiotic-resistant bacteria isolated from burn patients, *Burns*, 41, 7, 1488-1497, **2015.**

6. ACKNOWLEDGEMENTS

The authors would like to thank “Iran National Science Foundation (INSF)” for supporting this work under grant number 93032025.